JOURNAL OF MATERIALS SCIENCE 21 (1986) 2435–2440

Heterogeneous nucleation of crazes below notches in glassy polymers

R. P. KAMBOUR, M. A. VALLANCE, E. A. FARRAYE, L. A. GRIMALDI*
*Polymer Physics and Engineering Branch and *Materials Characterization Operation, Corporate Research and Development, General Electric Company, Schenectady, New York 12301, USA*

A slip-line field study of craze initiation at plastic zone tips below notches in polycarbonate has been carried out over a wide temperature range. Combination of the critical values of hydrostatic tension with Yee's temperature data for bulk modulus leads to a calculated critical elastic dilation in the region beyond the zone tip that is nearly temperature-independent. Microscopic investigation, however, shows strong evidence that crazes in polycarbonate and other glassy resins initiate at micrometre-size foreign particles. Assuming that the foreign particle is a rigid adherent sphere, a stress analysis for the particle situated on the elastic side of the elasto-plastic boundary has been effected; the particle is found to raise the hydrostatic tension over the value in the homogeneous field by 104%. In view of this analysis the polycarbonate experimental results suggest a temperature-independent, critical local elastic dilation of greater than 2% as a crazing criterion. Based on these results it may be suspected that all crazes – surface or internal – in glassy polymers, except at crack tips, are heterogeneously nucleated at impurity sites.

1. Introduction

Deformation of notched specimens of so-called ductile glassy polymers causes plane-strain shear flow from the notch. Eventually, a craze forms at the tip of the shear zone. On further loading the craze breaks and brittle fracture ensues. Assuming ideal plastic–rigid behaviour the stresses at the point of craze nucleation have been calculated using slip-line plasticity theory [1–7]. For a wide range of plastics these stresses (specifically, the major principal stress σ_{yy} and the hydrostatic tension p) have been correlated with the same compound parameter that serves to correlate the critical applied stress for surface crazing, namely $\Delta T \cdot \mathrm{CED}$ [8], where $\Delta T = T_g - T_{test}$ and CED is the resin cohesive energy density.

This paper reports further studies of internal crazing that have now been carried out in the hope of laying a basis for a comprehensive model of the initiation process.

2. Results

2.1. Temperature dependence of initiation resistance

Notched bars of Lexan* BPA polycarbonate extruded sheet each containing a machined notch 2 mm deep of root radius $\varrho = 0.50$ mm were tested in a three-point bend test with a 6 cm span as before [8]. Tests were conducted from below $-110°$ C (where brittle failure from the notch surface intervened) to above 80° C (where plastic collapse of the specimen began) at a crosshead rate of 0.02 in. min^{-1} (0.5 mm min^{-1}). Specimens were removed after craze initiation, sectioned and polished as before. The position of craze initiation, assumed to be the source of the curved growth lines [8] (Fig. 1), was determined in each case and its distance x to the notch base recorded. From the dependence of the yield stress on temperature (Fig. 2), x and ϱ, values of σ_{yy} and p for initiation were calculated (Figs 2 and 3). In Fig. 4 values of the dynamic bulk modulus K' at 1 Hz, calculated from the dynamic Poisson's ratio [10, 11], are displayed against temperature over the same temperature range. The temperature dependence of the nominal elastic dilation Δ at initiation has been calculated by dividing the smoothed $p(T)$ data in Fig. 3 by the smoothed $K'(T)$ data of Fig. 2; the resulting Δ is displayed against temperature in Fig. 3.

2.2. Microscopy of the initiation site

Notched three-point bend specimens of several of the resins employed in the previous study [8] were deformed to the point of fracture. Examination of the fracture surface revealed a "mirror" area having the shape and size of the craze formed prior to fracture. A pattern of curved lines, each meeting the border of the mirror area at right angles and all radiating from a common origin in the mirror area, were seen in the surface topography. These lines are believed to be the remnants of the growth lines seen in the unbroken craze. After metallizing this pattern of lines was still evident upon scanning electron microscope (SEM) examination. The radiating lines were thus used as a map that enabled identification of the craze nucleation site by SEM.

Specimens of several resins were enclosed in polyethylene bags (for cleanliness), loaded to fracture and

*Registered trademark of the General Electric Company.

0022–2461/86 $03.00 + .12

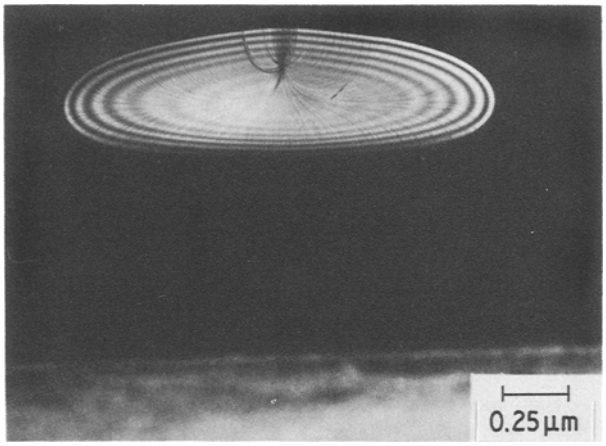

Figure 1 Craze at tip of plastic zone showing curved growth lines emanating from initiation site. Reflected colimated monochromatic light [8].

then removed from the bags just prior to metallization and inspection. Scanning micrographs of several of the initiation sites are shown in Figs 5 to 9. The initiation sites either contain what appear to be "foreign" particles of the order of a micrometre in size or else display a filamentary morphology suggestive of resin being ripped away from the surface of a foreign particle.

Energy-dispersive X-ray scans of these particles frequently indicated the presence of the element silicon (e.g. perhaps as silicates) in greater concentration than in the surrounding resin. In another case (Fig. 9) the particle was found to contain high levels of copper, iron and sulphur.

The presence of rigid foreign particles – actually found or inferred from resin damage – at many of these initiation sites suggests that nucleation may occur via (a) cavitation in the resin near the particle, (b) debonding from the particle surface followed perhaps by expansion of the hole all around the particle, or (c) fracture of the foreign particle itself. For the moment we term all these possibilities "heterogeneous nucleation mechanisms".

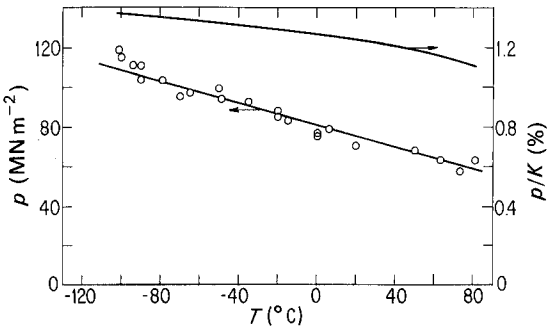

Figure 3 Temperature dependence of hydrostatic tension p at craze initiation (data) and the smoothed elastic dilation p/K' (line) for polycarbonate.

3. Theory

3.1. Modelling stress distributions at rigid foreign particles beyond the plastic zone tip: the adherent sphere

Dekkers and Heikens [12] have recently shown that in tensile bars crazing will initiate at the pole of an embedded sphere if the sphere is well bonded to the matrix and shear flow does not occur first. If the sphere is not bonded to the matrix a "cap" of resin/bead separation starts at the pole and spreads along the interface. At about 60° away from the pole the radial stress at the cap edge is no longer tensile, a so-called Poisson effect; further loading produces a craze radiating outwards from this position. The elastic analysis of stresses in the neighbourhood of an adhered rigid sphere in a linear elastic matrix subjected to remote uniaxial tension is well known [13]. This analysis calculates the hydrostatic tension to be maximum at the pole of the spherical inclusion, suggesting a correlation between volume dilation and craze nucleation [12].

Any triaxial stress state that is remote from the inclusion can be referenced to the principal stress coordinate system. In this case the state of stress appears as three orthogonal normal stresses. The state of stress in the elastic region beyond the elastic–plastic boundary of the plastic zone below a notch is such a case. For the case of linear elasticity, the local

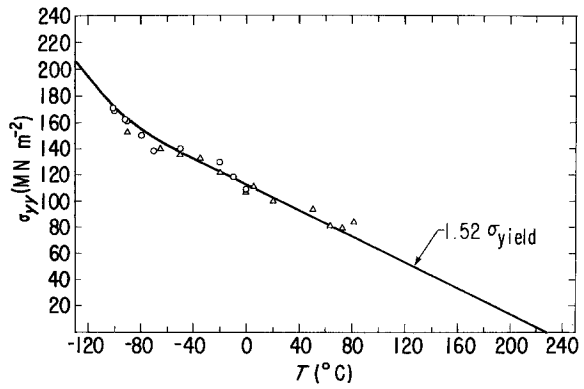

Figure 2 Temperature dependence of the major principal stress σ_{yy} at craze initiation (data) and tensile yield stress Y [9] (line) in polycarbonate; dY/dT scaled empirically to fit σ_{yy} data.

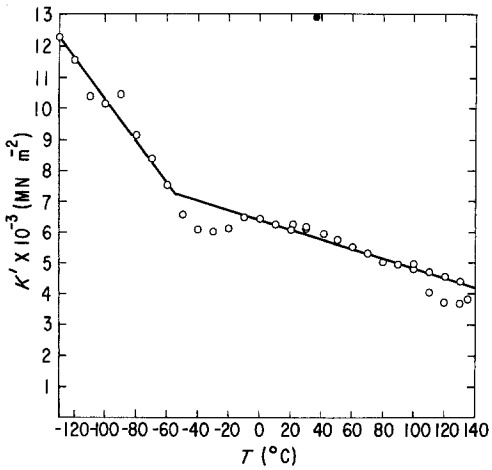

Figure 4 Temperature dependence of the dynamic bulk modulus K' for polycarbonate. Data of Yee [10].

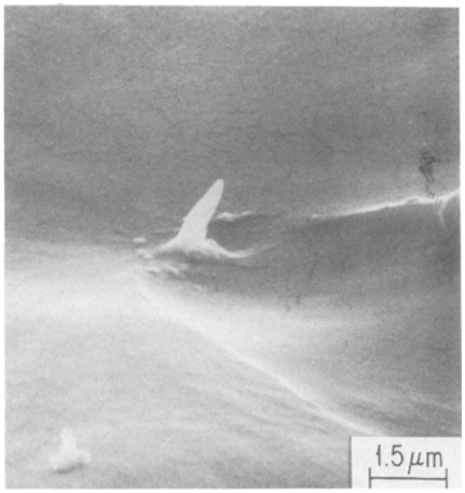

Figure 5 Craze initiation site in a specimen of BPA polycarbonate extrudate. Scanning electron micrograph.

stresses at a spherical inclusion are expressed by superimposing Goodier's solution [13] three times.

A notation is adopted wherein $\Phi_1 = 0$ is aligned with the first principal stress; $\Phi_1 = \pi/2$, $\theta_1 = 0$ is aligned with the second; and $\Phi_1 = \pi/2$, $\theta_1 = \pi/2$ with the third. Three local coordinate systems are defined: Φ_i, θ_i with $i = 1$, 2 or 3. The second principal stress direction corresponds to $\Phi_2 = 0$ and the third to $\Phi_3 = 0$. Inspection of the geometry leads to the following relationships:

$$\tan \Phi_2 = \frac{(\cos^2 \Phi_1 + \sin^2 \Phi_1 \sin^2 \theta_1)^{1/2}}{\sin \Phi_1 \cos \theta_1}$$

$$\tan \theta_2 = \frac{\cos \Phi_1}{\sin \Phi_1 \sin \theta_1}$$

$$\tan \Phi_3 = \frac{(\cos^2 \Phi_1 + \sin^2 \Phi_1 \cos^2 \theta_1)^{1/2}}{\sin \Phi_1 \sin \theta_1)}$$

$$\tan \theta_3 = \frac{\sin \Phi_1 \cos \theta_1}{\cos \Phi_1}$$

with $0 \leqslant \Phi_1, \theta_1 \leqslant \pi/2$. The Goodier solution for stress can be represented tensorially or as a 3×3 matrix $[\sigma(r/a, \Phi, S, G_2/G_1, \nu_1, \nu_2)]$ where r/a is the radial distance to the point of interest normalized by the radius of the spherical inclusion, S is the magnitude of the remotely applied uniaxial stress, G_2/G_1 is the ratio of the matrix shear modulus to that of the inclusion, and ν_1 and ν_2 are Poisson's ratios for the inclusion and matrix, respectively. The exact form of that solution is not reported here. If the inclusion is rigid, this reduces to $[\sigma(r/a, \Phi, S, \nu_2)]$. The stress solution for the triaxial state of remote stress is

$$\sum (r/a, \Phi_1, \theta_1, S_1, S_2, S_3, \nu_2) = [C_1] \times \left\{ \sum_{i=1,2,3} [C_i]^T [\sigma(r/a, \Phi_i, S_i, \nu_2)][C_i] \right\} [C_1]^T$$

where S_1, S_2 and S_3 are the principal stresses remote from the inclusion and T designates matrix transposition. Let $\boldsymbol{e}_1$, $\boldsymbol{e}_2$ and $\boldsymbol{e}_3$ be unit vectors in the S_1, S_2 and S_3 directions, respectively, and let $\boldsymbol{i}_i$, $\boldsymbol{j}_i$ and $\boldsymbol{k}_i$ be unit vectors directed along the orthogonal, curvilinear coordinates corresponding to r, Φ_i and θ_i. Then $[C_i]$ is defined as

$$\begin{bmatrix} \boldsymbol{i}_i \\ \boldsymbol{j}_i \\ \boldsymbol{k}_i \end{bmatrix} = [C_i] \begin{bmatrix} \boldsymbol{e}_1 \\ \boldsymbol{e}_2 \\ \boldsymbol{e}_3 \end{bmatrix}$$

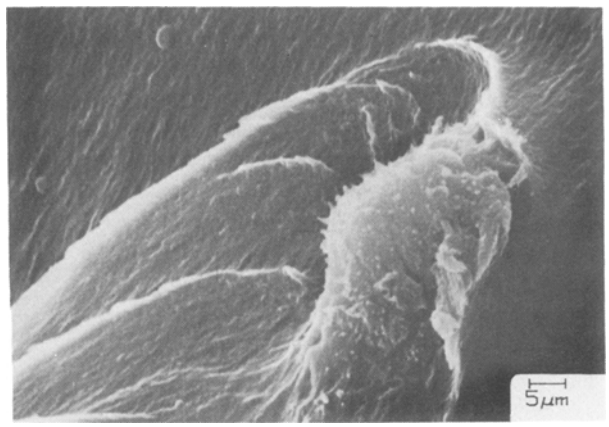

Figure 7 Craze initiation site in a specimen of BPA phthalate/carbonate copolymer injection moulding.

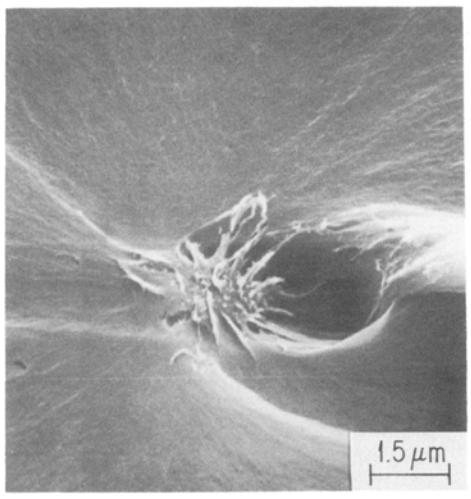

Figure 6 Craze initiation site in a specimen of polyetherimide extrudate.

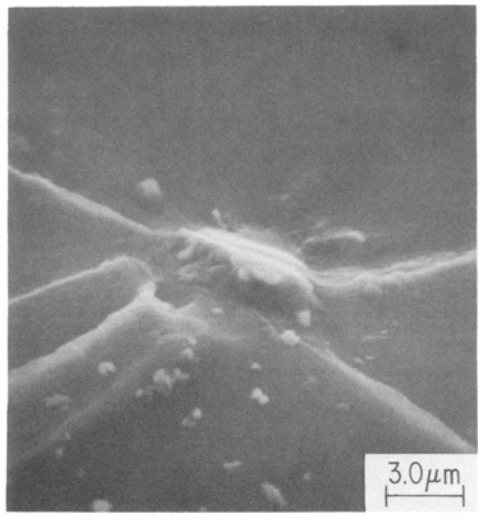

Figure 8 Craze initiation site in a specimen of polyetherimide compression moulding.

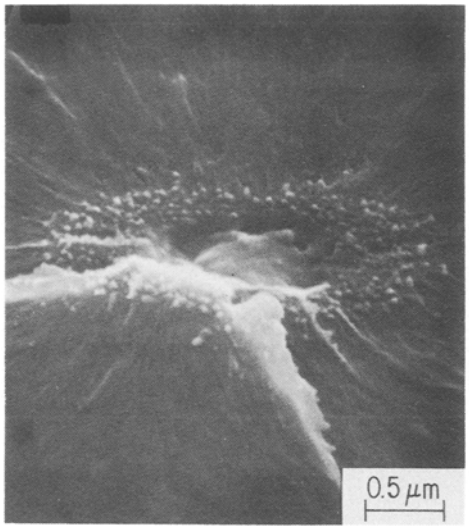

Figure 9 Craze initiation size in a specimen of poly(2,6-dimethyl-1,4-phenylene oxide) compression moulding.

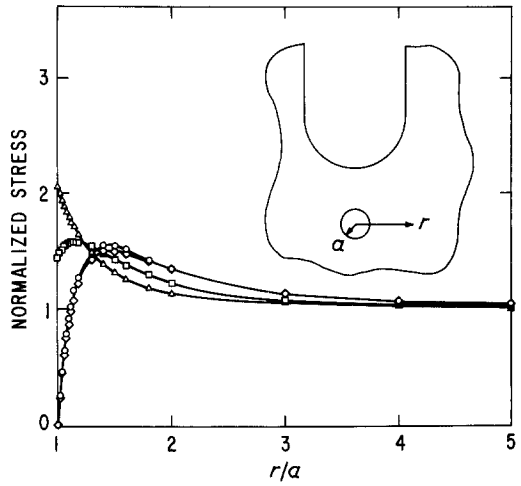

Figure 10 Normalized stress profiles at the pole ($\Phi = 0$) against normalized distance from the centre of a rigid adherent sphere embedded on the elastic side of the elastoplastic boundary of the sub-notch plastic zone. a = sphere radius. (○) τ/τ_{ff}, (△) p/p_{ff}, (□) $\sigma_r/\sigma_{r,ff}$, (◇) $\tau_m/\tau_{m,ff}$.

For instance

$$[C_1] = \begin{bmatrix} \cos\Phi_1 & \sin\Phi_1\cos\theta_1 & \sin\Phi_1\sin\theta_1 \\ -\sin\Phi_1 & \cos\Phi_1\cos\theta_1 & \cos\Phi_1\cos\theta_1 \\ 0 & -\sin\theta_1 & \cos\theta_1 \end{bmatrix}$$

Once the sum has been calculated at a point (r/a, Φ_1, θ_1), the principal stresses at that point are the three solutions to the polynomial equation

$$\left(\sum_i\right)^3 = I_1\left(\sum_i\right)^2 + I_2\sum_i - I_3 = 0$$

where I_i are the scaler invariants of the stress state at that point. Maximum shear stress, octahedral shear stress and hydrostatic tension are calculated in a straightforward manner. This mathematical development forms the basis of an algorithm programmed in BASIC 3.0 for use on a Hewlett-Packard 220 personal computer.

To use the algorithm in the present case, it has been assumed that the inclusion is embedded in the elastic region just beyond the elastic–plastic boundary directly beneath the notch tip. It is from this region that the craze is seen to initiate. The stresses in the plastic zone are calculated according to the statically determinate, incompressible, ideal plastic–rigid, plane-strain Hill [14] solution. It is assumed that no characteristic lines cross the elastic–plastic boundary more than once. The rigid assumption asserts that elastic strains must be negligible relative to the plastic strains in the system. The Hill solution gives the stresses directly beneath the notch as

$$S_1 = 2k\left[1 + \ln\left(1 + \frac{x}{\varrho}\right)\right]$$

$$S_2 = 2k\left[\frac{1}{2} + \ln\left(1 + \frac{x}{\varrho}\right)\right]$$

$$S_3 = 2k\left[\ln\left(1 + \frac{x}{\varrho}\right)\right]$$

where k is related to the yield stress in tension Y by $k = Y/3^{1/2}$, ϱ is the notch radius and x is the distance beneath the notch. In the present analysis x is taken as the distance to the craze nucleus. In order that the state of stress be equal across the elastic–plastic boundary, the elastic material must be incompressible, an automatic corollary of the rigid assumption. For consistency the value of v_2 in the Goodier analysis will be taken as 0.5. The authors realize that this is an imprecise value for v_2, which is to a degree contradictory to the small-strain dilation data presented earlier. The Goodier solution is not particularly sensitive to changes in v_2 over the range 0.35 to 0.5. This assumption of incompressibility is probably minor when compared to the assumption of linear elastic response implicit in the Goodier solution.

The analysis just described has been used to calculate the local matrix stresses in the region of an adhered, rigid, spherical inclusion subjected to the three-dimensional stress field existing beneath the notch at the craze nucleation site in BPA polycarbonate at 23° C. For that case, the remote principal stresses are all tensile in the ratios 2.45 : 1.73 : 1. It is found that octahedral shear stress τ is maximum for values of Φ_1 from 40 to 50°, depending on θ_1. For uniaxial tension τ is maximum at 45°. For uniaxial tension and for the stress field beneath the notch, hydrostatic tension P is maximum and τ is minimum at $\Phi = 0$ at the interface between the rigid sphere and the matrix. The stress profiles as functions of distance from the interface are given for $\Phi = 0$ in Fig. 10, which shows p, τ, maximum shear stress $\tau_m = (\sigma_1 - \sigma_3)/2$ and adhesive or radial normal stress σ_r. All are normalized by their far-field values. Of the four stresses only p is maximum at the interface. The shear stresses and the radial stress show maxima some distance away.

The highest level of τ occurs for $\Phi_1 = 45°$, $\theta_1 = 90°$. A similar plot is shown for stress drop-off in that direction in Fig. 11. The hydrostatic tension p has an unusually flat profile in that direction while the initial gradient of τ for $r/a < 1.2$ is the same as in Fig. 11, but opposite in sign. The high values of τ (and of τ_m) observed here suggest another difficulty with the

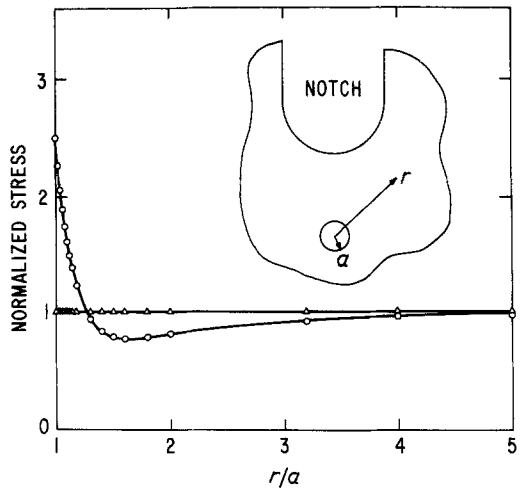

Figure 11 Normalized stress profiles 45° from pole at $\theta_1 = 90°$ for same sphere as in Fig. 10. (○) τ/τ_{ff}, (△) p/p_{ff}.

analysis. The far-field stresses used in the analysis are those predicted at the elastic–plastic boundary where τ is at the yield limit $(2Y/3)^{1/2}$. There the shear-stress concentrations caused by the spherical inclusion would cause local yielding to occur at certain locations near the inclusion. For this reason, the elastic analysis must be considered as a rough approximation of the stresses near the embedded inclusion. The analysis, none the less, is very useful for discussing certain observed phenomena.

When the far-field value of τ reaches the yield stress, a large region surrounding the embedded sphere undergoes yielding. In most circumstances, depending upon the nature of the constraint, regional yielding leads to shear flow, a very effective mechanism for stress relief and strain-energy dissipation. The inclusion is essentially disarmed as a nucleation site for crazing.

On the other hand, when stress concentration (such as that at an embedded rigid sphere) results in yielding over a very small region which is surrounded and constrained by elastic material, minimal plastic deformation occurs. Although stress redistribution may occur, the inclusion may still be a concentrator of dilational stress. Since cavitation must be a strong function of hydrostatic tension, it is of interest to compare the values of p_{lm}/τ_{ff} for the different geometries being discussed, where the subscript lm indicates local maximum and ff indicates far field. This ratio is of more interest than p_{lm}/τ_{lm} for the reasons cited. Presumably, large ratios correspond to increased probabilities of cavitation preceding gross shear flow. Results of the analysis for a rigid spherical inclusion embedded in a uniaxial tensile field and in the triaxial tensile field of interest are summarized in Table I. The ratio p_{lm}/τ_{ff} is 0.707 for uniaxial tension with no inclusion, 2.92 in the triaxial tension yield beneath the notch, 4.24 at the interface of an embedded sphere in a uniaxial tensile bar, and 5.97 at the interface of an embedded sphere in the triaxial tensile field beneath the notch.

A limited number of three-point bend tests of notched polycarbonate specimens containing isolated glass beads 0.1 mm in diameter bonded to the resin with γ-aminopropyl triethoxy silane produced craze

TABLE I Calculated stress ratios

Material	Ratio calculated*	Uniaxial tension	Plastic zone below root of notch
No inclusion	p/τ	0.707	2.92(+313%)
Embedded, rigid, adherent sphere	p_{lm}/τ_{ff}	4.24(+500%)	5.97(+745%)
	p_{lm}/τ_{lm}	1.96(+177%)	2.39(+228%)
	τ_{lm}/τ_{ff}	2.16(+116%)	2.50(+150%)

*p = hydrostatic tension, τ = octahedral shear stress, subscript lm = local maximum value found on sphere interface, subscript ff = far field value. Figures in brackets are percentage increases in ratio above value for uniaxial tension with no inclusion.

initiation at $\Phi_1 = 0$ on the beads. Notched bending tests of neat polycarbonate produce crazes from interior nucleation sites which for the most part seem to be inorganic inclusions. Tensile tests of smooth bars of polycarbonate in air at similar strain rates result in failure by necking. Inclusion of adhered glass beads in these tensile tests [15] has also resulted in failure by necking although shear flow is first seen emanating from the spherical interface at $\Phi_1 = 45°$. These observations agree with the trends predicted analytically.

4. Discussion

That foreign particles embedded in the matrix may nucleate crazes has been recognized for nearly forty years [16]. It has apparently not been widely appreciated that almost all bulk plastic specimens fabricated to date have very likely contained a sufficient concentration of foreign particles of the size discussed in Section 2.2 to provide a craze nucleating site for at least every cubic millimetre of resin. (For example 10^{-7} vol % of particles each of linear dimension 1 μm is sufficient.) The exceptions may be certain ultraclean specimens produced in a vacuum system by bulk polymerization of distillable monomers using distillable initiators [17].

Moreover, the fact that the same materials correlation serves to unify both the crazing resistance below notches and the surface-craze initiation resistance for all glassy polymers [8] suggests the possibility that so-called surface-craze initiation in smooth surfaces may be heterogeneously nucleated by embedded foreign particles as well.

Major details of the nucleation mechanism remain obscure at present. That Δ for polycarbonate is nearly independent of temperature (Fig. 3) lends appeal to a critical dilation criterion.

Moreover, p_{lm} at the pole of a rigid adherent spherical particle beyond the plastic zone tip at the notch is of the order of 100% greater than p_{ff} in the same region (Table I: 5.97/2.92 = 2.04). This suggests that Δ_{lm} is 2.04 Δ_{ff}, that is, Δ for polycarbonate (Fig. 3) is greater than 2%. It does not seem very likely that this level of dilation is great enough to bring about a spontaneous void nucleation *in* the resin adjacent to the interface (i.e. a mechanism that might be called a localized but homogeneous one). It is more likely that crazes nucleate by a true heterogeneous mechanism, with elastic dilation acting to produce debonding from the particle and the resultant interfacial microcrack

then producing craze growth into the resin by the menicus instability mechanism [18].

If cavitation occurs predominantly in the adjacent resin then the CED dependence is immediately obvious. However, a case can be made for a CED-correlated debonding mechanism as well: the work of adhesion of a liquid of low surface tension γ_L on a solid of high surface tension (e.g. most inorganic dirt) is proportional to γ_L. In turn γ_L is linearly dependent on the CED for most organic liquids.

Pinpointing the most promising directions for further study of the nucleation mechanism is uncertain for several reasons. Foremost is the problem of choosing for deliberate incorporation a particle representative in all important respects of the foreign particles that most often produce craze nucleation in commercial plastics – respects such as size, shape, internal strength and degree of adhesion to the matrix. Second is the lack of sufficient knowledge about shear deformation in a patch of resin bonded to the particle surface. Third is the lack of knowledge about the hydrostatic stress–dilation behaviour of resins at high stresses: can a homogeneous cavitational instability occur at stresses of the magnitude realized at foreign particles? Or as a practical matter, does all nucleation occur by true interfacial failure?

Whatever the future course of understanding at present it appears possible that all crazes produced to date, in uncracked, homogeneous glassy thermoplastics – both "surface" and interior crazes – may have initiated at impurity sites. If true, this likelihood will probably require to some degree the reinterpretation of all previous experimental studies of craze initiation – especially stress-state studies.

Acknowledgements

We wish to express our gratitude to A. F. Yee for the use of his unpublished dynamic bulk modulus data and to J. M. Kelly for his assistance in fabricating and testing specimens containing glass beads.

References

1. N. J. MILLS, *J. Mater. Sci.* **11** (1976) 363.
2. M. ISHIKAWA, I. NARISAWA and H. OGAWA, *J. Polym. Sci., Polym. Phys. Edn.* **15** (1977) 1791.
3. I. NARISAWA, M. ISHIKAWA and H. OGAWA, *Phil. Mag.* **A41** (1980) 331.
4. *Idem, J. Mater. Sci.* **15** (1980) 2059.
5. M. ISHIKAWA, H. OGAWA and I. NARISAWA, *J. Macromol. Sci.-Phys.* **B19** (1981) 421.
6. M. ISHIKAWA and I. NARISAWA, *J. Mater. Sci.* **18** (1983) 1947.
7. *Idem, ibid.* **18** (1983) 2826.
8. R. P. KAMBOUR and E. A. FARRAYE, *Polym. Commun.* **25** (1984) 357.
9. J. C. BAUWENS, *J. Mater. Sci.* **7** (1972) 577.
10. A. F. YEE, unpublished results (1985).
11. *Idem, Amer. Chem. Soc. Polym. Prep.* **22**(2) (1981) 285.
12. M. E. J. DEKKERS and D. HEIKENS, *J. Mater. Sci.* **18** (1983) 3281.
13. J. N. GOODIER, *Trans. ASME* **55** (1953) 39.
14. R. HILL, "Mathematical Theory of Plasticity" (Clarendon Press, Oxford, 1950) p. 245.
15. M. E. J. DEKKERS and D. HEIKENS, *J. Mater. Sci.* **19** (1984) 3271.
16. B. MAXWELL, private communication (1985).
17. T. KAINO, K. JINGUJI and S. NARA, *Appl. Phys. Lett.* **41** (1982) 802.
18. A. S. ARGON and M. M. SALAMA, *Mater. Sci. Eng.* **23** (1977) 219.

Received 29 July
and accepted 18 September 1985